

PRINCIPLES OF X-RAY MAGNETIC DICHROISM SPECTROMICROSCOPY

J. STÖHR

*IBM Research Division, Almaden Research Center,
650 Harry Road, San Jose, CA 95120, USA*

H. A. PADMORE, S. ANDERS and T. STAMMLER

*Advanced Light Source, Lawrence Berkeley National Laboratory,
1 Cyclotron Road, Berkeley, CA 94720, USA*

M. R. SCHEINFEIN

*Department of Physics and Astronomy, Arizona State University,
Tempe AZ 85287-1504, USA*

Received 4 June 1998

A review is given of the principles underlying X-ray magnetic circular (XMCD) and linear (XMLD) dichroism spectromicroscopies consisting of polarized X-ray absorption spectroscopy in conjunction with scanning or imaging microscopy. The techniques are shown to have many useful and important capabilities for the study of complex magnetic materials. They offer elemental specificity, chemical specificity and variable depth sensitivity, among others. XMCD microscopy is best suited for the study of ferromagnets and ferrimagnets, and it allows a quantitative determination of the size and direction of spin and orbital moments. XMLD microscopy promises to become a powerful tool for the study of antiferromagnets which are difficult to study by conventional microscopy techniques.

1. Introduction

The ability to control thin film growth at the atomic level has led to a renaissance in research on magnetism and magnetic materials during the last decade. The renaissance is partly driven by the interesting physics of these complex, often layered, materials and it is clearly fueled by the magnetic storage industry with worldwide revenues exceeding US\$50 billion per year. As illustrated in Fig. 1, structures containing artificially layered magnetic and nonmagnetic thin films are the foundation of magnetic recording heads and disks used in today's computers.¹ Ever-increasing storage needs drive the miniaturization of all components, in particular the size of the recording heads and the size of the stored bits on the disk. Magnetic storage technology is predicted to continue its domination in the next decade or so. Magnetic materials may even have applications in computer memory, the holy grail of semi-

conductor devices. Magnetic memory cells, where the 1 and 0 bits correspond to different orientations of nonvolatile magnetic domains,^{2,3} pose a challenge to conventional dynamic random access memory (DRAM) and may well be used in tomorrow's computers. The extensive use of hard and soft magnets in electric power production and utilization also contributes to the motivation for research into new magnetic materials.

Advances in growth of increasingly sophisticated and interesting magnetic nanostructures require advances in experimental probes that are sensitive to the compositional and magnetic microstructure. Desired capabilities are elemental, chemical and structural sensitivities over a wide range of spatial dimensions, lateral and depth, coupled with a sensitivity to the size and orientation of the magnetic moments. XMCD spectromicroscopy, first demonstrated in 1993,^{4,5} offers many of these capabilities.

Magnetic Technologies in Computers

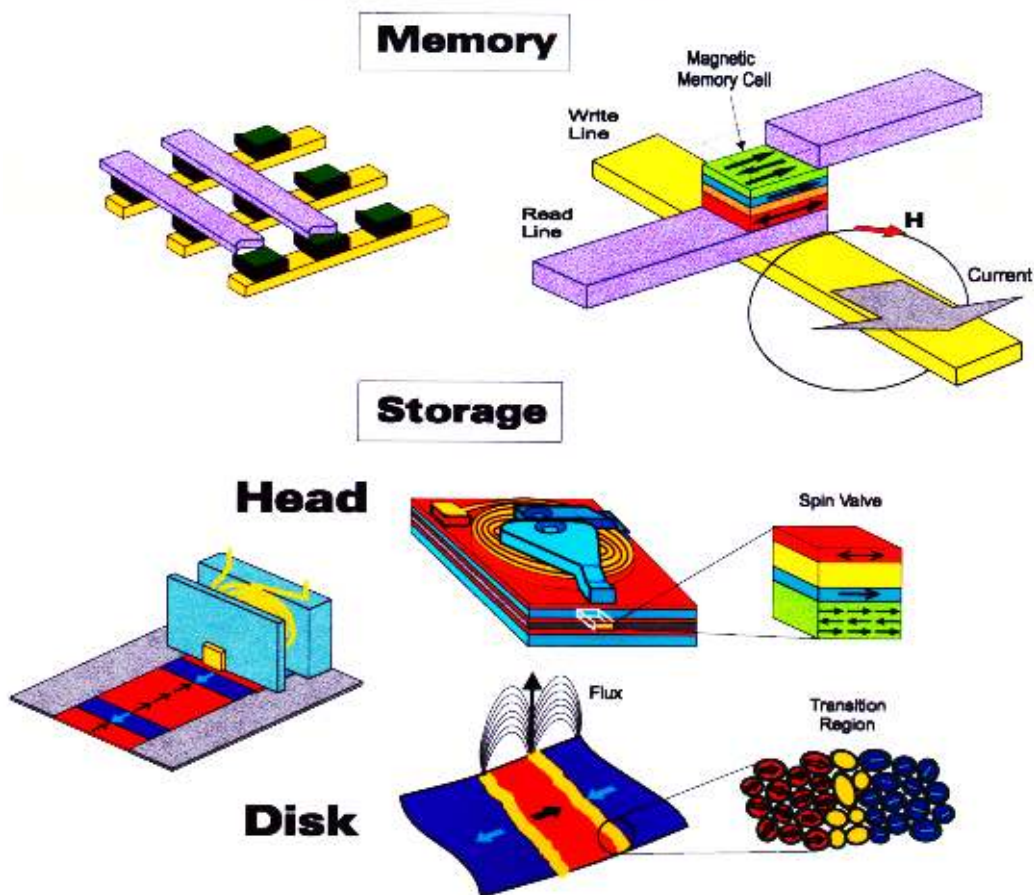


Fig. 1. Illustration of various applications of magnetic devices in computers. In magnetic memory cells the 1 and 0 bits correspond to different magnetization directions in the red layer. The bit is written by the magnetic field surrounding the current in a write line. The bit is read by a current flowing through the cell, either a spin valve³ or tunnel valve.⁴³ Through a change in resistance the current senses whether the magnetization directions in the blue and red ferromagnetic layers are aligned parallel or antiparallel. The most advanced magnetic read heads are spin valves, consisting of two ferromagnetic layers (red and blue) separated by a nonmagnetic layer (yellow). The blue layer is pinned by exchange coupling to an antiferromagnet shown in green. The spin valve senses, through the giant magnetoresistive effect, the direction of the magnetic flux emerging from the magnetic domains of a recording disk which rotates underneath. The magnetic flux rotates the magnetization direction in the red layer relative to the fixed direction in the blue layer. The flux density is highest at the transition regions between the magnetic bits and depends on the width of the transition regions. The width is kept small by using a granular magnetic alloy in which the grains are partially decoupled from each other by nonmagnetic skins containing elements like B or Ta.

XMLD spectromicroscopy has only recently been demonstrated⁶ and from our present understanding⁷⁻¹⁰ it is safe to predict that this technique will offer many exciting opportunities in the future. Here we discuss the principles underlying the two techniques. Particular emphasis is given to the microscopy method that is most closely related to low energy electron microscopy (LEEM), namely X-ray photoelectron emission microscopy (X-PEEM). This

technique combines secondary electron imaging with scanning of the photon energy to obtain spectroscopic contrast.

2. Principles of XMCD and XMLD Spectroscopy

Spectromicroscopy combines the principles of spectroscopy with those of microscopy.¹¹ In this section we shall review the spectroscopy aspects.

X-ray Absorption Spectroscopy

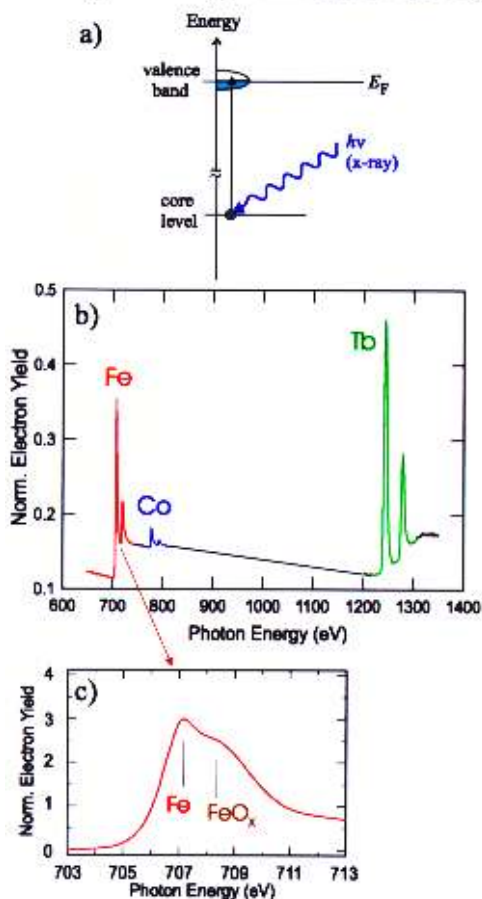


Fig. 2. (a) Principles of X-ray absorption spectroscopy, using a one-electron model for the case of L edge absorption in a d band transition metal.¹⁴ In the X-ray absorption process an electron is excited from the core shell to empty valence states. This results in pronounced resonances at the absorption thresholds, as illustrated in (b) for the $2p_{3/2} \rightarrow 3d$ (L_3 edge) and $2p_{1/2} \rightarrow 3d$ (L_2 edge) excitations in Fe and Co and the $3d_{5/2} \rightarrow 4f$ (M_5 edge) and $3d_{3/2} \rightarrow 4f$ (M_4 edge) excitations in Tb. Here the X-ray absorption spectrum for a $\text{Tb}_{24.5}\text{Fe}_{70.5}\text{Co}_{5.0}$ alloy is shown, recorded by means of total electron yield detection. The L edge resonances for Fe and Co and the M edge resonances for Tb are indicated in different colors. (c) Fine structure of the Fe L_3 resonance in a partially oxidized Fe thin film, illustrating the chemical specificity of X-ray absorption spectroscopy.

Some of the most powerful spectroscopy methods are based on the absorption of photons, since this process is guided by simple electronic dipole transitions. X-rays offer the advantage over visible light that the spectroscopy becomes element-specific.

The elemental specificity arises from the characteristic binding energies of the atomic core electrons as illustrated in Fig. 2(a). X-ray absorption (XAS) and X-ray photoelectron spectroscopy (XPS) are the two most widely used core electron spectroscopies. In the following we shall discuss only XAS and its application for microscopy. The choice of XAS over XPS is based on several reasons. XAS is the simpler technique in terms of instrumentation, it is less demanding with respect to photon flux and, most important, it can probe samples in a bulk-sensitive (transmission) or surface-sensitive (electron yield detection) mode, which is of great importance for artificially made multilayer structures. The X-ray absorption spectrum directly exhibits the characteristic absorption edges of the elements in the sample, as shown in Fig. 2(b) for a $\text{Tb}_{24.5}\text{Fe}_{70.5}\text{Co}_{5.0}$ alloy. At the absorption thresholds of the elements the spectrum shows strong resonances arising from transitions to unfilled valence band states. Since the transitions are governed by the $\Delta l = \pm 1$ selection rule, the d band transition metals are best studied using $L_{2,3}$ edges ($2p \rightarrow d$) and the rare earths using $M_{4,5}$ edges ($3d \rightarrow 4f$), as shown in Fig. 2(b) for Fe and Co ($L_{2,3}$ edges) and Tb ($M_{4,5}$ edges). X-ray absorption spectroscopy is also sensitive to the chemical environment, similar to XPS, as shown in Fig. 2(c), where the fine structure of the L_3 edge of an oxidized Fe film is shown.

In practice, X-ray absorption spectroscopy is carried out with polarized synchrotron radiation. Use of the X-ray polarization enables studies of the electronic and magnetic anisotropies of a sample. The polarization characteristics of synchrotron radiation from a bending magnet source are illustrated in Fig. 3. If the beam line only accepts radiation through a horizontal slit positioned in the plane of the electron storage ring, the X-rays are linearly polarized as shown in red on the right side of the figure. Linearly polarized light can be described by a biaxial electric field vector. If, instead, the horizontal aperture is placed below the orbit plane of the ring, the electrons in the ring appear to rotate counterclockwise and the resulting electron angular momentum is transferred to the emitted photon, as shown in the middle panel of Fig. 3. The transmitted radiation is right-circularly-polarized (RCP). For RCP photons the electric field vector \mathbf{E} of the X-ray rotates counterclockwise about the X-ray emission direction \mathbf{k} if

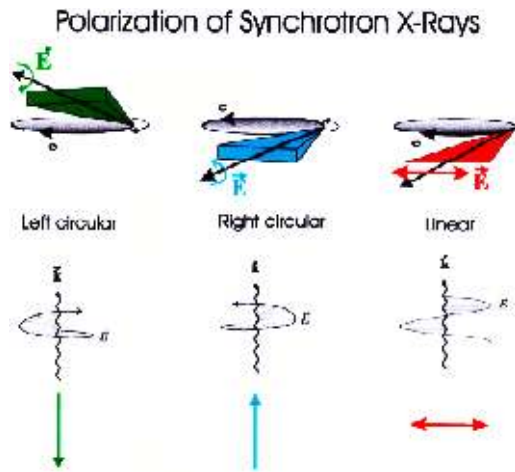


Fig. 3. Origin of polarized synchrotron radiation from a bending magnet source. If radiation in the plane of the electron orbit is selected by a suitable aperture, linearly polarized radiation is obtained as illustrated on the right side of the figure. By selecting radiation below or above the orbit plane, right- or left-handed circularly polarized radiation is obtained, as explained in the text. Linear polarization can be described by a biaxial vector and handed circular polarization by a vector, the photon spin.

viewed toward the source, and clockwise if viewed in the direction of \mathbf{k} . RCP photons carry an angular momentum $+\hbar$ and can be characterized by a vector, the photon spin, which by definition is in the direction of \mathbf{k} .¹² The opposite senses of electron and electric field vector rotations apply for an aperture placed above the plane of the storage ring, as shown on the left side of Fig. 3, and left-circularly-polarized (LCP) photons are obtained in this case.

The simple description of the photon polarization by a biaxial vector for linear polarization and a vector for handed circular polarization is the physical basis for probing various anisotropies of the sample. In general, linearly polarized light can only detect an anisotropy of the electronic charge, i.e. its quadrupole moment which is related to the square of the electron angular momentum. In contrast, handed circularly polarized light can measure a dipolar or vector quantity, in our case the size and direction of the electron angular momentum and spin.

2.1. XMCD spectroscopy

The concepts of XMCD spectroscopy, pioneered by Schütz *et al.*,¹³ are illustrated in Fig. 4 for a d tran-

sition metal. Here we have assumed that the d shell has a spin moment which is given by the imbalance of spin-up and spin-down electrons (states below the Fermi level, denoted as E_F) or, equivalently (except for a change of sign), by the imbalance of spin-up and spin-down holes (states above the Fermi level). In order to measure the difference in the number of d holes with up and down spin, we need to make the X-ray absorption process spin-dependent. This is done by use of RCP or LCP photons which transfer their angular momentum, $+\hbar$ and $-\hbar$, respectively, to the excited photoelectron. The photoelectron carries the transferred angular momentum as a spin or an angular momentum, or both.¹⁴ If the photoelectron originates from a spin-orbit-split level, e.g. the $p_{3/2}$ level (L_3 edge), the angular momentum of the photon can be transferred in part to the spin through the spin-orbit coupling. RCP photons transfer the opposite momentum to the electron from LCP photons, and hence photoelectrons with opposite spins are created in two cases. Since the $p_{3/2}(L_3)$ and $p_{1/2}(L_2)$ levels have opposite spin-orbit coupling ($l+s$ and $l-s$, respectively), the spin polarization will be opposite at the two edges. In the absorption process, “spin-up” and “spin-down” are defined relative to the photon helicity or photon spin. Since spin flips are forbidden in electric dipole transitions governing X-ray absorption, spin-up (spin-down) photoelectrons from the p core shell can only be excited into spin-up (spin-down) d hole states. Hence the spin-split valence shell acts as a detector for the spin of the excited photoelectron and the transition intensity is simply proportional to the number of empty d states of a given spin.

The quantization axis of the valence shell “detector” is given by the magnetization direction. The size of the dichroism effect scales like $\cos \theta$, where θ is the angle between the photon spin and the magnetization direction. Hence the maximum dichroism effect (typically 20%) is observed if the photon spin direction and the magnetization directions are parallel and antiparallel, as shown on the right side of Fig. 4. When the photon spin and the magnetization directions are perpendicular, the resonance intensities at the L_3 and L_2 edges lie between those obtained for parallel and antiparallel alignments.

The differences in the intensities at the L_3 and L_2 edges for parallel and antiparallel orientation of

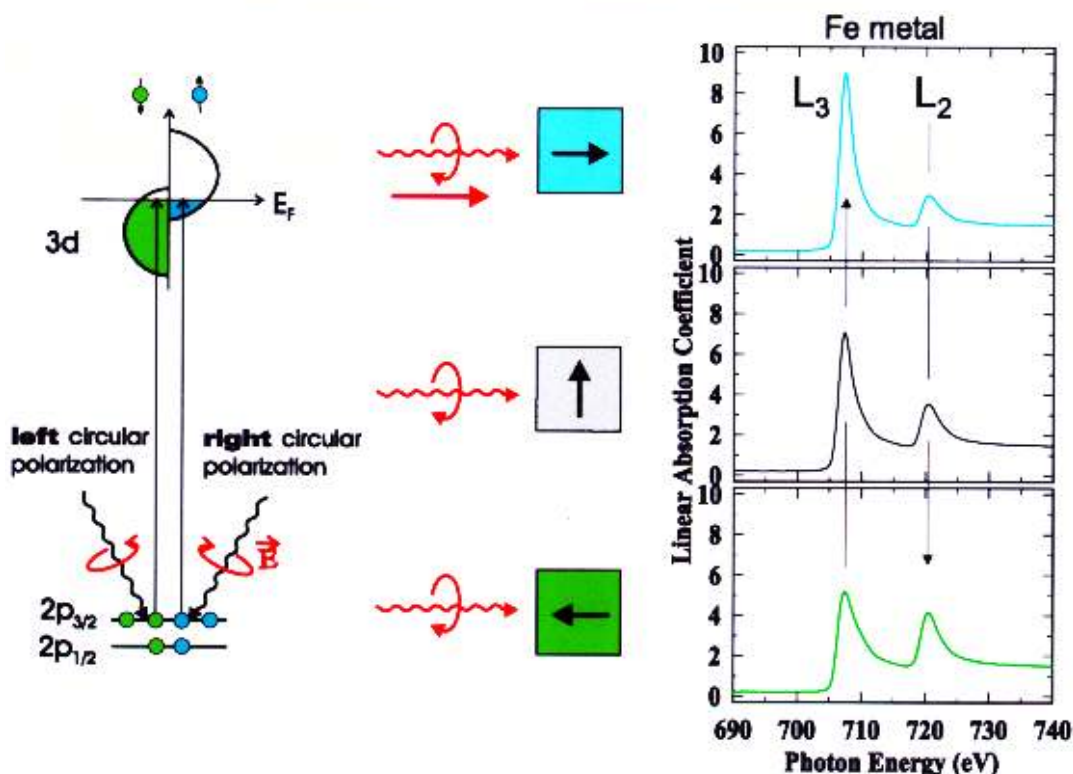
X-Ray Magnetic **Circular** Dichroism

Fig. 4. Principles of X-ray magnetic circular dichroism spectroscopy, illustrated for the case of L edge absorption in a d band transition metal. In a magnetic metal the d valence band is split into spin-up and spin-down states with different occupation. Absorption of right (left) circularly polarized light mainly excites spin-up (spin-down) photoelectrons. Since spin flips are forbidden in X-ray absorption, the measured resonance intensity directly reflects the number of empty d band states of a given spin. In XMCD spectroscopy it is equivalent whether the photon polarization is changed and the magnetization direction is kept fixed or whether the magnetization direction is changed and the photon helicity is fixed. The corresponding XMCD spectra for Fe metal⁴⁴ are shown on the right for three different orientations of the magnetization directions relative to the fixed photon spin (right circular polarization).

photon spin and magnetization directions are quantitatively related by sum rules to the size of the spin and orbital magnetic moments^{15,16} and to the anisotropies of the spin density and orbital moment.¹⁷ XMCD spectroscopy can therefore determine the sizes, the directions, and anisotropies (sizes in different directions) of the atomic magnetic moments.

2.2. XMLD spectroscopy

It is well known that linearly polarized X-rays can probe the orientation of molecular orbitals. This is one of the strengths of near edge X-ray absorption fine structure, (NEXAFS), spectroscopy.¹⁸ More generally, polarized X-ray absorption can sense the

charge anisotropy of the valence states involved in the core excitation process.^{19,20} The electric field vector \mathbf{E} of the linearly polarized X-rays acts as a searchlight for the number of valence holes in different directions of the atomic volume or the Wigner–Seitz cell. In most cases the anisotropy of the charge in the atomic volume is caused by an anisotropy in the bonding, i.e. by the electrostatic potential.

A lesser-known effect, which is the basis of XMLD spectroscopy, arises from the presence of a magnetic anisotropy in the sample.^{7–10} Let us consider the case of NiO. Because of the cubic symmetry of the lattice the charge distribution around the atoms is nearly spherical and no linear dichroism effect exists in the absence of magnetic

X-Ray Magnetic **Linear** Dichroism

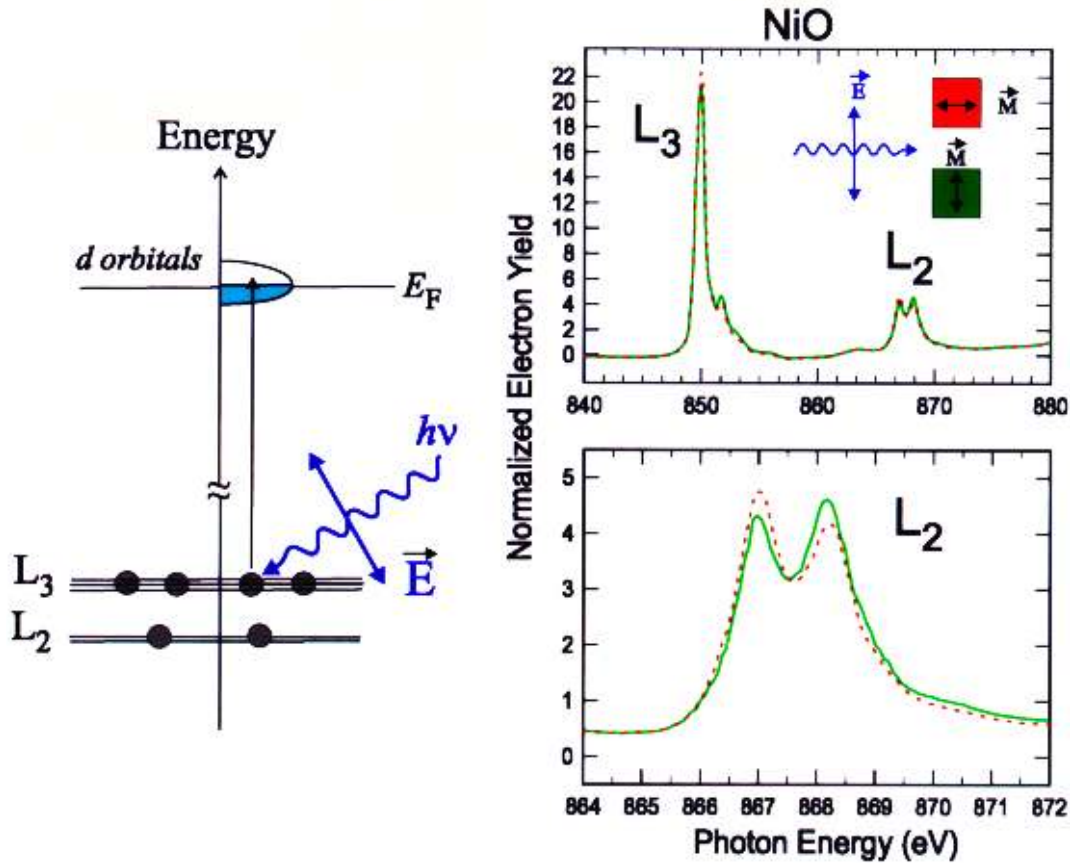


Fig. 5. Principles of X-ray magnetic linear dichroism spectroscopy, illustrated for NiO. In the X-ray absorption process core electrons are excited from the $2p$ shell to empty d states. The X-ray absorption spectrum of NiO exhibits additional fine structure at the L_3 and L_2 absorption edges arising from final state multiplet coupling of the $2p$ core hole with the d valence hole ($2p^53d^9$ configuration.⁴⁵) Both edges exhibit a linear dichroism effect for alignment of the \mathbf{E} vector parallel versus perpendicular to the magnetic axis. The spectra were recorded by surface-sensitive electron yield for a 45 nm-thick NiO(100) film grown on MgO(100). Near the surface the magnetic axis is preferentially perpendicular to the surface. The green curve corresponds to \mathbf{E} perpendicular to the surface and the red curve for \mathbf{E} parallel to the surface.

interactions. NiO is antiferromagnetic, however, and the Ni spins are oriented in the $(1, 1, 1)$ plane along the $[\sqrt{2}, 1, 1]$, $[1, \sqrt{2}, 1]$ or $[1, 1, \sqrt{2}]$ axes in the fcc lattice.²¹ There is no net magnetic moment, because an equal number of spins point to opposite directions, and so only a preferential magnetic axis exists. The alignment of the local atomic spins along this axis breaks the cubic symmetry of the charge through the spin-orbit coupling. As a consequence the charge exhibits a small anisotropy in the unit cell, i.e. it is no longer spherical but shows an ellipse-like distortion about the magnetic direction. This charge anisotropy leads to an asymmetry of the X-ray ab-

sorption signal through the searchlight effect. The maximum XMLD effect is obtained for \mathbf{E} parallel versus \mathbf{E} perpendicular to the magnetic axis. In contrast to the XMCD effect, the XMLD effect has a $\cos^2 \theta$ dependence, where θ is the angle between \mathbf{E} and the magnetic axis. In general, the XMLD effect is small in 3D metals owing to the small size of the spin-orbit interaction and the large band width, resulting in a small charge anisotropy when the d states are summed over the Brillouin zone. However, a sizeable XMLD effect (of order 10%) may be observed in the presence of multiplet splitting.^{9,10} Multiplet finestructure in the L_3 and L_2 resonances is

typically observed in transition metal compounds,²² as shown in Fig. 5 for the X-ray absorption spectrum of NiO. At a particular multiplet energy only selected *d* valence states are probed through matrix element effects that enhance the XMLD effect. In Fig. 5 the XMLD effect is especially visible at the Ni *L*₂ edge where a sizeable difference is observed for **E** parallel (green) versus perpendicular (red) to the magnetic axis.

3. Principles of XMCD and XMLD Microscopy

The two basic requirements for microscopy are spatial resolution and contrast. As for electron microscopy, one can use scanning or imaging to obtain spatial resolution. Three common experimental approaches are illustrated in Fig. 6. In the following we shall discuss the three methods in greater detail before summarizing the various contrast mechanisms.

3.1. Scanning X-ray microscopy

In scanning X-ray microscopy illustrated in Fig. 6(a) a monochromatic X-ray beam is focussed to the smallest possible spot size and the X-ray intensity transmitted through the sample, or the fluorescent X-ray or electron intensity from the sample is monitored as a function of the focussed beam position on the sample (either the sample or the beam position may be scanned).²³ In this approach the energy resolution is given by the monochromator in the beam line (not shown) and the spatial resolution is determined by the size of the X-ray spot. Small X-ray spots can be obtained by using the reflected and focussed beam from grazing incidence mirrors or the diffracted and focussed beam from a multilayer mirror or a zone plate. In practice, zone plate focussing, shown in Fig. 6(a), is yielding the smallest spot sizes. The focal spot size is determined by the width of the outermost zones of the zone plate²⁴ and today the resolution is typically about 50 nm, with expected resolutions near 20 nm in the future. Because the focal length of the zone plate lens changes with photon energy, for spectroscopic studies the sample position also needs to be scannable along the beam direction. X-ray transmission or fluorescent microscopies are well suited for studies in the presence of a magnetic

field, contrary to electron-based methods, and they are bulk-sensitive, as discussed below.

3.2. Imaging transmission X-ray microscopy

From an instrumental point of view, imaging transmission X-ray microscopy, shown in Fig. 6(b), is closely related to scanning X-ray microscopy, discussed above, since in both cases the spatial resolution is determined by zone plates.²⁴ Here a condenser zone plate in conjunction with a pinhole (typically with a 10–20 μm diameter) creates a monochromatic photon spot on the sample. The energy resolution is determined by the zone plate dimensions, and the pinhole size and is typically $\Delta E/E = 1/250$. It is about an order of magnitude worse than in scanning X-ray microscopy and in X-PEEM, discussed below. A micro-zone-plate generates a magnified image of the sample onto a phosphor screen or X-ray-sensitive CCD camera. The spatial resolution is determined by the width of the outermost zones of the micro-zone-plate,²⁴ and to date resolutions of 24 nm have been obtained.²⁵ Spectroscopic studies require movement of the condenser zone plate. The method is well suited for studies in the presence of magnetic fields and such studies have been performed by Fischer *et al.*^{26,27}

3.3. Imaging X-ray photoelectron microscopy

The second imaging method is based on X-rays-in/electrons-out and was pioneered by Tonner.²⁸ It is illustrated in Fig. 6(c). The sample is illuminated by a monochromatic X-ray beam that is only moderately focussed, for example to tens of micrometers, so that it matches the maximum field of view of a photoelectron microscope. The energy resolution is determined by the X-ray monochromator in the beam line and the spatial resolution is determined by the electron optics in the PEEM. It is limited by three quantities: spherical aberration, chromatic aberration and diffraction. In practice, for X-ray excitation of electrons chromatic aberrations dominate.^{28,29} They originate from errors in the focussing of electrons with different kinetic energies.

Most PEEM microscopies do not incorporate an energy analyzer or filter³⁰ and the detected electrons

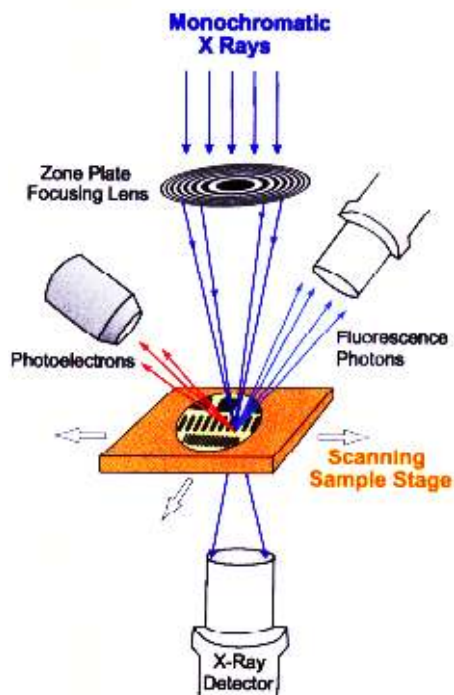
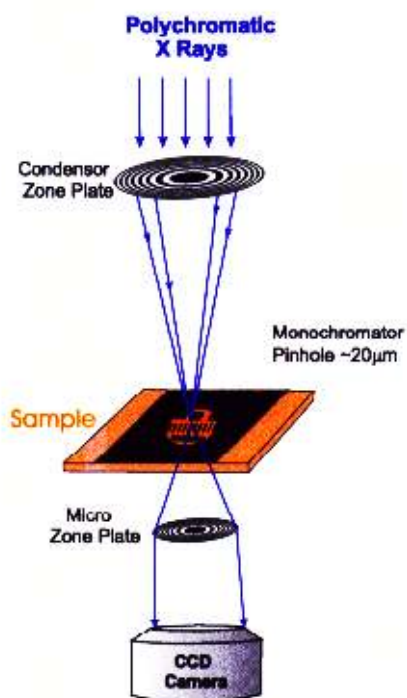
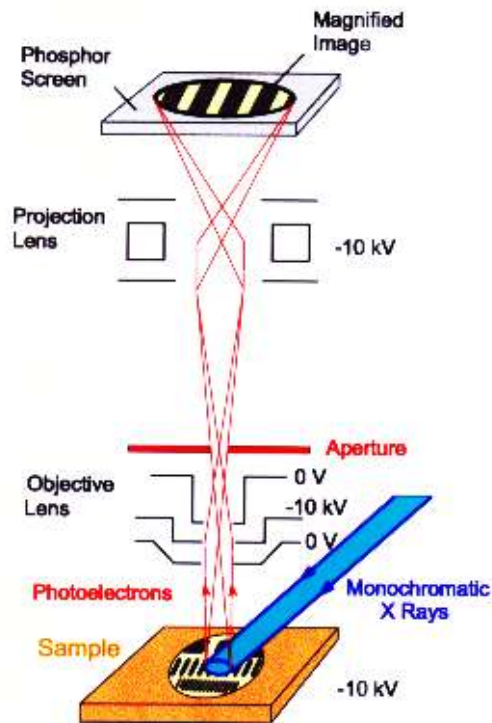
(a) Scanning X-ray Microscopy**(b) Imaging Transmission X-ray Microscopy****(c) Imaging X-Ray Photoelectron Microscopy**

Fig. 6. Principles of scanning X-ray microscopy, shown in (a), and two imaging X-ray microscopy techniques, shown in (b) and (c). In the scanning mode (a) a small X-ray spot is formed by a suitable X-ray optic, for example a zone plate as shown, and the sample is scanned relative to the X-ray focal spot. The spatial resolution is determined by the spot size. The intensity of the transmitted X-rays or the fluorescence or electron yield from the sample are detected as a function of the sample position and thus determine the contrast in the image. In imaging transmission X-ray microscopy, shown in (b), a condenser zone plate in conjunction with a pinhole before the sample produces a monochromatic photon spot on the sample. A micro-zone-plate generates a magnified image of the sample which can be viewed in real time by an X-ray-sensitive CCD camera. The spatial resolution is determined by the width of the outermost zones in the micro-zone-plate. In imaging X-ray photoelectron microscopy, shown in (c), the X-rays are only moderately focused in order to match the field of view of an electron microscope. Electrons emitted from the sample are projected with magnification onto a phosphor screen and the image can be viewed in real time at video rates. The spatial resolution is determined by the electron optics within the microscope, the size of the aperture and the operation voltage.

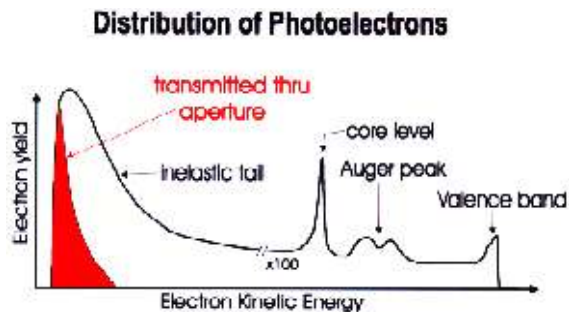


Fig. 7. (a) Schematic illustration of the photoelectron energy distribution from the sample after X-ray excitation. The photoemission spectrum is dominated by the low energy, scattered electrons (inelastic tail). The aperture in the backfocal plane of the PEEM shown in Fig. 6(c) leads to an electron-energy-filtering effect, so that only the electron intensity shown in red is transmitted.

are mostly low energy secondary electrons, as illustrated in Fig. 7. X-ray excitation produces photoelectrons with a characteristic energy distribution. The electron intensity is dominated, by orders of magnitude, by the secondary electron tail in the 0–20 eV kinetic energy range, where zero kinetic energy corresponds to the vacuum level of the sample.³¹ The secondary electron signal, which closely follows the X-ray absorption spectrum of the sample,³¹ determines the X-PEEM intensity and resolution. Its large intensity provides a suitably large PEEM signal, but the energy spread of the inelastic tail (about 5 eV for most materials³²) spoils the resolution through chromatic aberrations.

Fortunately, the effective width of the energy spread is reduced by a suitable aperture placed in the back focal plane of the PEEM, as shown in Fig. 6(c). This is illustrated in Fig. 7 for the case where the microscope is designed to accept only the lowest energy electrons, corresponding to optimum spatial resolution. The aperture acts as a filter for high energy electrons which are focussed behind the aperture while the low energy portion of the inelastic tail is properly focussed at the aperture position and is thus transmitted. The transmitted portion is schematically shown in red in Fig. 7. Calculations show that a spatial resolution in the 10–20 nm range can be obtained by X-PEEM because of the energy filtering effect of the aperture.³³ Even better spatial resolutions are achieved when the energy spread of the emitted electrons is reduced. This situation is en-

countered when ultraviolet radiation is used with an energy slightly higher than the work function and a spatial resolution of 8 nm has been demonstrated.³⁴ In this case chromatic aberrations are strongly reduced by the narrow width of the secondary electron distribution. At X-ray energies 22 nm spatial resolution has been achieved by the use of an energy filter to reduce the electron energy spread.³⁵ In the future lateral resolutions near 2 nm appear possible by use of aberration-correcting optics.³⁶

3.4. Contrast mechanisms

The intensity changes with photon energy or X-ray polarization discussed in the earlier spectroscopy section naturally lend themselves as contrast mechanisms for scanning and imaging X-ray microscopy. For example, if the photon energy is tuned to 707 eV, the L_3 resonance of Fe metal (see Fig. 2), the measured signal from the sample will emphasize Fe over other elements in the sample. If we change the

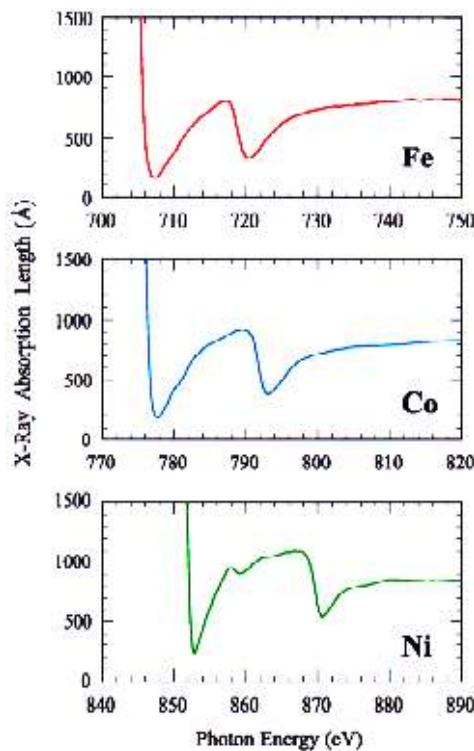


Fig. 8. X-ray absorption length ($1/e$ attenuation) for Fe, Co and Ni in the L edge region.³⁷ The absorption lengths in the pre-edge regions (not shown) are about 600 nm.

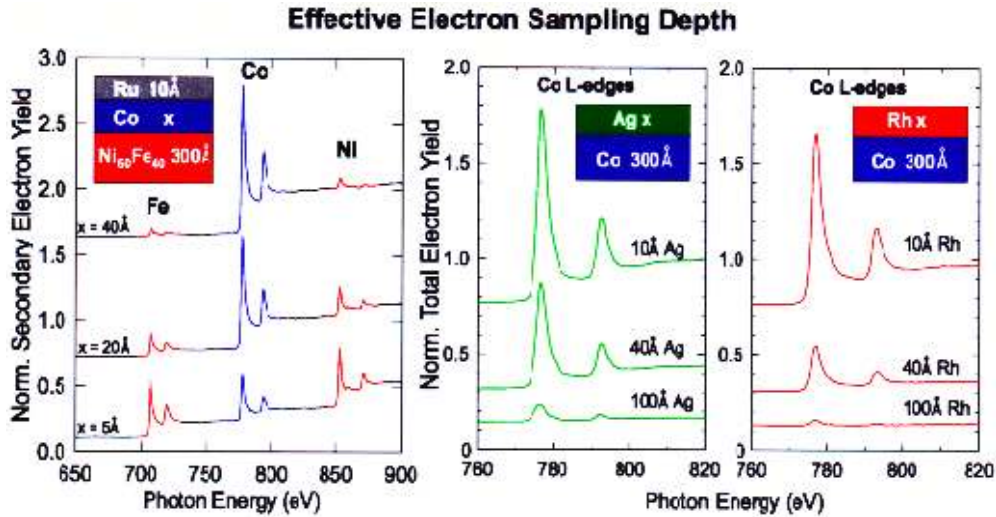


Fig. 9. Illustration of the effective secondary electron sampling depth in various metal multilayers as discussed in the text.

polarization from linear to circular, Fe regions in the sample will be emphasized whose magnetization direction is parallel to the photon spin (see Fig. 4). It is not necessary in many cases to change the photon spin in XMCD microscopy, since the contrast is large and can be enhanced by combining images recorded at the L_3 and L_2 edges.

For antiferromagnets the photon energy of the linearly polarized light is tuned to a particular multiplet peak, such as one of the L_2 edge peaks in Fig. 5. Domains with an orientation of the magnetic axis parallel to \mathbf{E} will then show a different intensity than those with the axis perpendicular to \mathbf{E} . Again the contrast can be enhanced by combining images taken at different photon (multiplet) energies.

In addition to the spectroscopic contrast, other basic contrast mechanisms exist. In X-PEEM the electron yield from different sample areas is also determined by the local work function and topology. In transmission X-ray microscopy additional contrast arises from differences in the X-ray absorption coefficient at nonresonant photon energies caused by compositional changes or thickness variations of the sample.

3.5. Surface versus bulk sensitivity

X-ray transmission microscopy samples the average absorption along the photon path. In the soft X-ray region the $1/e$ absorption length is typically of

the order 100 nm, but it varies greatly near the absorption edges due to resonance effects. This is illustrated in Fig. 8 for the metals Fe, Co and Ni. At the L_3 edges the X-ray absorption length is only about 15–20 nm.³⁷ In order to avoid saturation effects, for quantitative measurements the sample should not be thicker than about two to three times the X-ray absorption length.³⁸ For practical sample thicknesses of 50 nm or more, surface effects are typically negligible and X-ray transmission microscopy is therefore bulk-sensitive.

In contrast, the X-PEEM signal originates closer to the sample surface. The sampling depth is determined by the cascading process of the scattered Auger electrons created after core excitation. The $1/e$ sampling depth is about 1.7 nm for Fe and 2.5 nm for Co and Ni.³⁷ Figure 9 illustrates the practical sampling depth for several multilayer samples. For example, it is seen that the signal from a $\text{Ni}_{60}\text{Fe}_{40}$ layer buried under a 4 nm Co plus 1 nm Ru layer can still be seen. The figure also shows results for a Co layer buried under Ag or Rh capping layers. The escape depth, which is largely determined by scattering processes from filled to empty d states and scales inversely with the number of d holes,³⁹ is longer in Ag (~ 4.1 nm) than in Rh (~ 2.5 nm). The Co signal is still clearly visible through a 10 nm Ag layer. As a rule of thumb one can still “see” layers that are buried as deep as three times the $1/e$ sampling depth.

4. Conclusions

XMCD and XMLD spectromicroscopies are shown to offer many useful and important capabilities for the study of ferromagnets, ferrimagnets and antiferromagnets. In comparison to the many other magnetic microscopy techniques, like Kerr microscopy, spin-polarized LEEM, scanning electron microscopy with polarization analysis (SEMPA), Lorentz microscopy and magnetic force microscopy (MFM), to name a few, the X-ray techniques offer some unique advantages, such as elemental and chemical contrast, variable depth sensitivity and the ability to study antiferromagnets.

Relative to the other techniques, however, XMCD and XMLD microscopies are still in their infancy. Although many examples of “test patterns” have been published,^{4,5,26,27,40,41,42} the challenge clearly lies in impacting the field of magnetic phenomena and materials. One may identify three important length scales for magnetic imaging which consecutively decrease by factors of 100. The first one is about 1 μm , set by the size of lithographically fabricated magnetic cells such as in spin valve heads or magnetic memory cells. The second one is about 10 nm, corresponding to the crystallographic grain size of typical magnetic materials. The final one is 0.1 nm, the atomic size. Impact can occur on all three length scales, but even for the largest length scale one would like to have a spacial resolution of 0.1 μm . To date only the best X-PEEM instruments therefore have sufficient resolution. Advances in instrumentation remain a challenge.

Acknowledgments

This research was supported by the Laboratory Technology Research Partnership Program, Office of Energy Research, US Department of Energy, under a CRADA (Cooperative Research and Development Agreement) between Lawrence Berkeley National Laboratory and IBM, Almaden, and by the Office of Energy Research, Office of Basic Energy Sciences, of the US Department of Energy, under contract No. DE-AC03-76SF00098. Experimental results presented in this paper were obtained at the Stanford Synchrotron Radiation Laboratory, which is operated by the US Department of Energy.

References

1. For a review see *IBM J. Res. Develop.* **42**, 3 (1998).
2. J. M. Daughton, *Thin Solid Films* **216**, 162 (1992).
3. D. Tang *et al.*, *IEEE Trans. Mag.* **31**, 3206 (1995).
4. J. Stöhr *et al.*, *Science* **259**, 658 (1993).
5. C. M. Schneider *et al.*, *Appl. Phys. Lett.* **63**, 2432 (1993).
6. D. Spanke *et al.*, *Phys. Rev.* **B58**, 5201 (1998).
7. B. T. Thole, G. van der Laan and G. A. Sawatzky, *Phys. Rev. Lett.* **55**, 2086 (1985).
8. G. van der Laan *et al.*, *Phys. Rev.* **B34**, 6529 (1986); G. van der Laan and B. T. Thole, *Phys. Rev.* **B43**, 13401 (1991).
9. P. Kuiper *et al.*, *Phys. Rev. Lett.* **70**, 1549 (1993).
10. D. Alders *et al.*, *Europhys. Lett.* **32**, 259 (1995).
11. Sometimes the term “spectromicroscopy” is used only for true imaging techniques such as PEEM, while the term “microspectroscopy” is used for scanning techniques.
12. The handedness of circularly polarized light is not uniquely defined. We follow Feynman and the convention used in particle physics. See R. P. Feynman, R. B. Leighton and M. Sands, *The Feynman Lectures on Physics*, Vol. I, Part 2 (Addison-Wesley, Reading, 1964).
13. G. Schütz *et al.*, *Phys. Rev. Lett.* **58**, 737 (1987).
14. J. Stöhr and Y. Wu, in *New Directions in Research with Third-Generation Soft X-Ray Synchrotron Radiation Sources*, eds. A. S. Schlachter and F. J. Wuilleumier (Kluwer, Netherlands, 1994), p. 221.
15. B. T. Thole, P. Carra, F. Sette and G. van der Laan, *Phys. Rev. Lett.* **68**, 1943 (1992).
16. P. Carra, B. T. Thole, M. Altarelli and X. Wang, *Phys. Rev. Lett.* **70**, 694 (1993).
17. J. Stöhr and H. König, *Phys. Rev. Lett.* **75**, 3748 (1995).
18. J. Stöhr, *NEXAFS Spectroscopy*, Vol. 25 of *Springer Series in Surface Sciences* (Springer, Heidelberg, 1992).
19. P. Carra, H. König, B. T. Thole and M. Altarelli, *Physica* **B192**, 182 (1993).
20. J. Stöhr, *J. Electron Spectrosc. Rel. Phenom.* **75**, 253 (1995).
21. S. Saito, M. Miura and K. Kurosawa, *J. Phys.* **C13**, 1513 (1980).
22. F. M. F. de Groot, *J. Electron Spectrosc. Relat. Phenom.* **67**, 529 (1994).
23. J. Kirz and H. Rarback, *Rev. Sci. Instrum.* **56**, 1 (1985).
24. For reviews on X-ray transmission microscopy see J. Kirz, C. Jacobsen and M. Howells, *Quarterly Rev. Biophys.* **28**, 1 (1995), and G. Schmahl, D. Rudolph, B. Niemann, P. Guttman, J. Thieme and G. Schneider, *Naturwissenschaften* **83**, 61 (1996).
25. G. Schneider, T. Schliebe and H. Aschoff, *J. Vacuum Sci. Technol.* **B13**, 2809 (1995).
26. P. Fischer *et al.*, *Z. Phys.* **101**, 313 (1996).
27. P. Fischer *et al.*, *J. Phys.* **D31**, 649 (1998).

28. B. P. Tonner and G. R. Harp, *Rev. Sci. Instrum.* **59**, 853 (1988).
29. B. P. Tonner, D. Dunham, T. Droubay and M. Pauli, *J. Electron Spectrosc Rel. Phenom.* **84**, 211 (1997).
30. Instruments with energy filters have been used by Schneider *et al.*,⁵ Tonner *et al.*,²⁹ Fink *et al.*,³⁶ and Schmidt *et al.* (this issue).
31. J. Stöhr, in *X-Ray Absorption: Principles, Applications, Techniques of EXAFS, SEXAFS and XANES*, eds. D. C. Koningsberger and R. Prins (Wiley and Sons, New York, 1988), p. 443.
32. B. L. Henke, J. A. Smith and D. A. Attwood, *J. Appl. Phys.* **48**, 1852 (1977).
33. S. Anders, M. Scheinfein, R. Duarte, A. Cossy, T. Renner, H. Padmore and J. Diaz, LBNL report (unpublished).
34. G. F. Rempfer, W. P. Skoczylas and O. H. Griffith, *Ultramicroscopy* **36**, 196 (1991).
35. Th. Schmidt, S. Heun, J. Slezak, J. Diaz, K. C. Prince, G. Lilienkamp and E. Bauer (this issue).
36. R. Fink *et al.*, *J. Electron Spectrosc Rel. Phenom.* **84**, 231 (1997).
37. R. Nakajima and J. Stöhr and I. Idzerda (to be published).
38. P. A. Lee, P. H. Citrin, P. Eisenberger and B. M. Kincaid, *Rev. Mod. Phys.* **53**, 769 (1981).
39. H. C. Siegmann, *J. Phys.: Condens. Matter* **4**, 8395 (1992).
40. B. P. Tonner *et al.*, *Nucl. Instrum. Methods* **A347**, 142 (1994).
41. C. M. Schneider *et al.*, *Synchr. Rad. News* **10**, 23 (1997).
42. C. M. Schneider, *J. Mag. Mag. Mat.* **175**, 160 (1997).
43. J. S. Moodera, L. R. Kinder, T. M. Wong and R. Meservey, *Phys. Rev. Lett.* **74**, 3273 (1995).
44. C. T. Chen *et al.*, *Phys. Rev. Lett.* **75**, 152 (1995).
45. G. van der Laan, B. T. Thole, G. A. Sawatzky and M. Verdaguer, *Phys. Rev.* **B37**, 6587 (1988).